Isomerism Effects in the Collisional Excitation of Cyanoacetylene by Molecular Hydrogen

Cheikh Bop, Fidel A Batista-Romero, Alexandre Faure, Ernesto Quintas-Sánchez, Richard Dawes, Francois Lique

Isomerism Effects in the Collisional Excitation of Cyanoacetylene by Molecular Hydrogen

Cheikh. T. Bop,[†] Fidel A. Batista-Romero,[†] Alexandre Faure,[‡] Ernesto Quintas-Sánchez,[¶] Richard Dawes,[¶] and François Lique[*,†]

[†]*LOMC- UMR 6294, CNRS-Université du Havre, 25 rue Philippe Lebon, BP 1123, F-76063 Le Havre, France.*

[‡]*Université Grenoble Alpes, CNRS, IPAG, 38000 Grenoble, France*

[¶]*Department of Chemistry, Missouri University of Science and Technology, Rolla, MO 65409, USA*

E-mail: francois.lique@univ-lehavre.fr

Abstract

Rotational excitation of the interstellar HC_2NC and HNC_3 molecules, two isomers of HC_3N, induced by collisions with H_2 is investigated at low collision energy using a quantum time-independent approach. The scattering calculations are based on new high-level *ab initio* 4-dimensional (4D) potential energy surfaces (PESs) computed at the explicitly-correlated coupled-cluster with single, double, and perturbative triple excitations [CCSD(T)-F12b] level of theory. The method of interpolating moving least squares (IMLS) was used to construct 4D analytical PESs. Rotationally inelastic cross sections among the low-lying rotational levels of HC_2NC and HNC_3 were obtained using a pure quantum close-coupling approach for total energies up to $\sim$ 100 cm^{-1}. The corresponding thermal rate coefficients were computed for temperatures ranging from 1 to 20 K. Propensity rules in favor of even Δj_1 transitions were found for both HC_2NC

and HNC_3 in collisions with para-$H_2(j = 0)$, j_1 being the rotational level of HC_2NC and HNC_3 molecules. The new rate coefficients were compared with previously published HC_3N–para-$H_2(j = 0)$ rate coefficients. As expected, differences were found, especially for the rate coefficients corresponding to $\Delta j_1 = 1$ transitions. Such a comparison confirms the importance of having specific collisional data for the different isomers of a molecule. The new rate coefficients will be crucial to improve the estimation of the HC_3N:HC_2NC:HNC_3 abundance ratio in the interstellar medium.

Keywords

Astrochemistry, van der Waals complexes, Energy transfer, Molecular processes, Quantum Scattering

1 Introduction

Cyanoacetylene (HC_3N) was first detected in the interstellar medium (ISM) in 1971. Turner[1] reported observations of the $1-0$ line towards Sgr B2. Since then, HC_3N has been detected in a great variety of astronomical environments from external galaxies, to Galactic interstellar clouds, star forming regions, and planetary atmospheres. Because of its low rotational constant and large dipole moment, HC_3N is considered as a very good thermometer and barometer in the ISM.[2,3]

Usually, cyanide compounds like HCN or HC_3N display structural isomerism. The abundance and behavior of cyanides and their isomers in cold molecular clouds, especially the prototypical HCN/HNC system, have been the subject of much interest in the past few years (see references below). Given the low temperature of these environments, apparent anomalies in relative isomer populations have raised many questions about possible synthesis mechanisms and the feasibility of paths to isomerisation.

In the case of HC_3N, four isomers [HC_2NC, $HCNC_2$, HNC_3 and C_2(H)CN] have been

found to be stable in the laboratory. Among them, the HC_2NC and HNC_3 isomers have been detected in the ISM[4,5] and in the circumstellar envelope IRC+10216.[6] Knowing the abundance of the different isomers can be a useful tool to explore the physical and chemical conditions in molecular clouds.[7] Hence, the accurate derivation of the abundance of the HC_3N, HC_2NC and HNC_3 isomers is of fundamental interest for constraining the nitrogen and carbon chain chemistry, especially in cold molecular clouds.

However, the full exploitation of the rotational spectra, especially those from emission, and the accurate derivation of molecular abundances require calculation of collisional rate coefficients of the detected molecules with the most abundant interstellar species. Collisional data are even crucially needed when the gas density is below the critical density for line excitation.[8] Without these data, only approximate estimates of the molecular column density are possible assuming local thermodynamic equilibrium (LTE), which is generally not a good approximation.[8] Recently, to that aim, Faure *et al.*[9] reported calculations for rotational excitation of HC_3N by collisions with H_2, the dominant collisional partner in the cold ISM. Calculations are based on the interaction potential of Wernli *et al.*[10] whose accuracy is checked against spectroscopic measurements of the HC_3N–H_2 complex.[9] The quantum coupled-channel approach was employed and complemented by quasi-classical trajectory calculations.

However, to the best of our knowledge, no collisional data exist for the other detected isomers. A simple approach would consist of using HC_3N rate coefficients for the interpretation of HC_2NC and HNC_3 interstellar spectra. However, recent studies have shown that isomerism effects can be important in collisional studies and that the collisional rate coefficients of the different isomers can differ significantly.[11–14] The most famous example is that of the HCN and HNC molecules. Indeed, both the magnitude and the propensity rules of the HCN and HNC rate coefficients are very different, so that the excitation of these two molecules in the ISM presents very different characteristics.[14] It is then important to provide actual rate coefficients for the HC_2NC and HNC_3 molecules. The dominant collisional part-

ner in cold molecular clouds where these two isomers were detected is molecular hydrogen (H_2).

Thus, in this work, we use new 4-dimensional (4D) potential energy surfaces (PESs) for the ground electronic state of the HC_2NC–H_2 and HNC_3–H_2 collisional systems to investigate the rotational excitation of HC_2NC and HNC_3 by H_2. Collisional cross sections for the low-lying rotational levels of both HC_2NC and HNC_3 in collision with para-H_2 (hereafter p-H_2), the main constituent of the low temperature interstellar gas, are reported for collision energies up to 100 cm^{-1}, yielding rate coefficients up to 20 K.

The paper is organized as follows: Section II and III detail the PESs and scattering calculations, respectively, and Section IV presents our results. Discussion and conclusions are given in Section V.

2 Potential energy surfaces

2.1 Electronic structure calculations

Prior to compute the PESs of the colliding systems, we had an insight into the relative energies of the detected isomers of the HC_3N molecules. We used a similar approach to that used by Nguyen *et al.*[15] that benchmarked the energy difference between the HCN and HNC isomers using a high level composite theoretical approach. Then, energies were determined from an additive decomposition including a number of terms such as the Hartree-Fock energy, as well as valence, core, and high-order dynamic correlation, all determined from coupled-cluster theory near the complete basis set limit. Smaller correction terms of Diagonal Born-Oppenheimer Correction (DBOC), relativistic, and spin-orbit were also added. Finally, the significant contribution of anharmonic zero-point vibrational energy was estimated using perturbation theory. The study by Nguyen *et al.*[15] established the energy difference between HCN and the less stable HNC isomer as 5212 $\pm$ 30 cm^{-1}. We followed a nearly identical protocol here, except using the explicitly-correlated version of coupled-

cluster theory [CCSD(T)-F12b],[16] and therefore consider our new results as benchmarks with similar per-atom uncertainties. The 0 K enthalpies of formation for HC_3N, HC_2NC, and HNC_3 were calculated as 374.59, 488.88, and 588.03 kJ/mol respectively. Thus, relative to the most stable HC_3N isomer, HC_2NC and HNC_3 are found 9554 and 17842 cm^{-1} higher in energy, respectively.

Then, we focused on the HC_2NC–H_2 and HNC_3–H_2 PESs. The geometries of the HC_2NC–H_2 and HNC_3–H_2 complexes are characterized by three θ_1, θ_2 and ϕ angles, and the distance R between the centers of masses of HC_2NC (HNC_3) and H_2. The polar angles of HC_2NC (HNC_3) and H_2 with respect to the z-axis that coincides with $\vec{R}$ are denoted, respectively, by θ_1 and θ_2, while ϕ denotes the dihedral angle between half-planes containing the HC_2NC (HNC_3) and H_2 bonds. The $\theta_1 = 0°$ and $\theta_2 = 0°$ geometry corresponds to the HH$\cdots$HCCNC and HH$\cdots$CCCNH complexes, respectively.

The bond distance for H_2 was fixed at $r_{HH} = 0.76665$ Å, the vibrationally averaged bond distance for para-hydrogen, $j_2 = 0$, j_2 being the rotational state of H_2. For HC_2NC (the more stable isomer), the equilibrium geometry is linear and the structure employed in this study was that derived by Botschwina *et al.*[17] (denoted semi-empirical) which is consistent with the observed rotational constants for several isotopomers. As also reported by Botschwina *et al.*,[17] the equilibrium geometry for the less stable HNC_3 isomer was found to be quasi-linear, with a nearly linear heavy-atom backbone, but with the H-atom bent significantly away from the backbone axis. Geometry optimization at the CCSD(T)-F12b/VTZ-F12 level[16,18] yields a value of 139.5° for the C-N-H angle. Figure 1 provides the complete set of fully relaxed geometric parameters. As a quasi-linear molecule, with only the light H-atom significantly off-axis, the maximum in the rovibrational ground-state probability density is expected to be found at linear geometry. Indeed, so far only a single rotational constant has been determined from the experimental data, thus it was decided to use an effective linear geometry in the interaction potential. To determine an effective linear structure for HNC_3, a constrained (held linear) geometry optimization was performed at the explicitly correlated

(AE)-CCSD(T)-F12b/CVQZ-F12 level,[16,18] where (AE) indicates that all electrons were included in the correlation treatment. The bond distances so obtained are given in Figure 1. Hence, both HC_2NC and HNC_3 were considered as rigid linear rotor in the PES calculations.

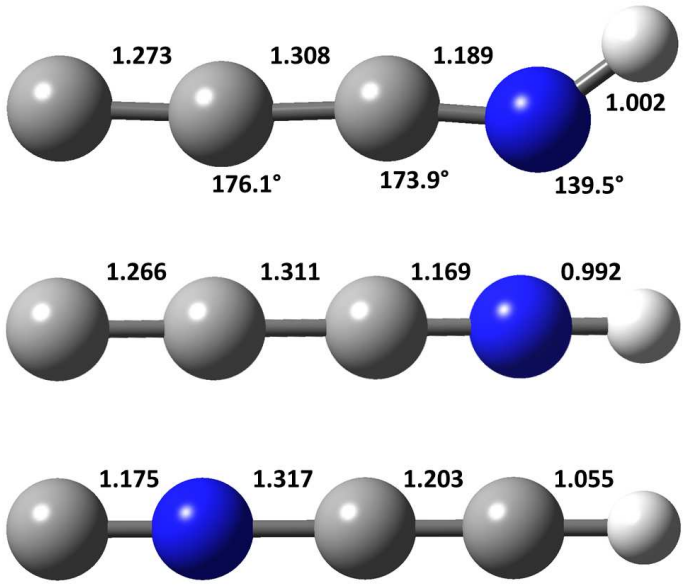

Figure 1: (Upper) Fully relaxed quasi-linear structure for HNC_3 optimized at the CCSD(T)-F12b/VTZ-F12 level. (Middle) Constrained linear structure for HNC_3 optimized at the (AE)-CCSD(T)-F12b/CVQZ-F12 level (see text). (Lower) Cemi-empirical structure of linear HC_2NC derived by Botschwina *et al.* (see text). Parameters are given in Angströms and degrees.

The Molpro electronic structure package was used to perform all of the calculations reported here.[19] 4D PESs were constructed for the two systems by fitting automatically–generated points at the CCSD(T)-F12b/VTZ-F12 level. For HC_2NC, two wells with similar depths are noted. First, a collinear structure with the H_2 molecule aligned end-on to the C-atom of HC_2NC, is found with a center-of-mass distance of 5.303 Å and a depth of 174.1 cm^{-1} relative to separated molecules. Second, a nearly parallel side-by-side structure is located with a slightly deeper well-depth of 178.0 cm^{-1}. The center-of-mass separation for this global minimum structure is 3.171 Å. For H_2 interacting with the (constrained) linear HNC_3, a deep well (467.9 cm^{-1}) corresponds to a side-on approach of the H_2 molecule to the H-atom end of the HNC_3 fragment, with a corresponding center-of-mass distance of 4.750 Å.

A much shallower well is found for end-on approach of H_2 to the C-atom end of the HNC_3 fragment (R = 5.359 Å and E = -270.8 cm^{-1}). The various minima can be seen in Figures 2 and 3.

The strength and anisotropy of the PES describing the interaction with collision partners govern the scattering dynamics and hence the derived cross sections, propensities and rate coefficients. For interactions of the neutral linear cyanide isomers with H_2 considered here, just as for HCN and HNC,[14] the relevant leading electrostatic terms are dipole-quadrupole and quadrupole-quadrupole. These interactions favor structural isomers of the complex that are either fully collinear (in the cases of HC_2NC and HNC_3 the H_2 aligns at the bare-C end of the cyanide), T-shaped arrangements with the H-end of the cyanide approaching the side of the H_2 molecule, or side-by-side parallel. For HC_2NC, all three arrangements are found as stable minima in the complex, with the collinear and side-by-side having similar well-depths that are slightly more stable than the T-shaped isomer. In the case of HNC_3, again all three structures appear as minima, but here the T-shaped well is by far the deepest (and much deeper than the wells of the HC_2NC system), while the collinear and side-by-side wells are shallower. The side-by-side wells for the two systems are similar in depth, but the increased depth of the T-shaped and collinear wells in the HNC_3 system corresponds to significantly greater anisotropy and range in the interaction potential, which impacts the computed scattering cross sections as is discussed next.

2.2 Analytical representation

4D PESs were constructed for the two isomeric systems using an automated interpolating moving least squares (IMLS) method. The method has been used in several previous studies[20–22] and is now being freely released as a software package under the name AUTOSURF.[23–25] The fitting basis and other aspects of the procedure were the same as described previously. The ranges of intermonomer center-of-mass distances are $R = [2.5, 22.0]$ and $R = [2.3, 22.0]$ Å for HC_2NC–H_2 and HNC_3–H_2 respectively. The global estimated root-

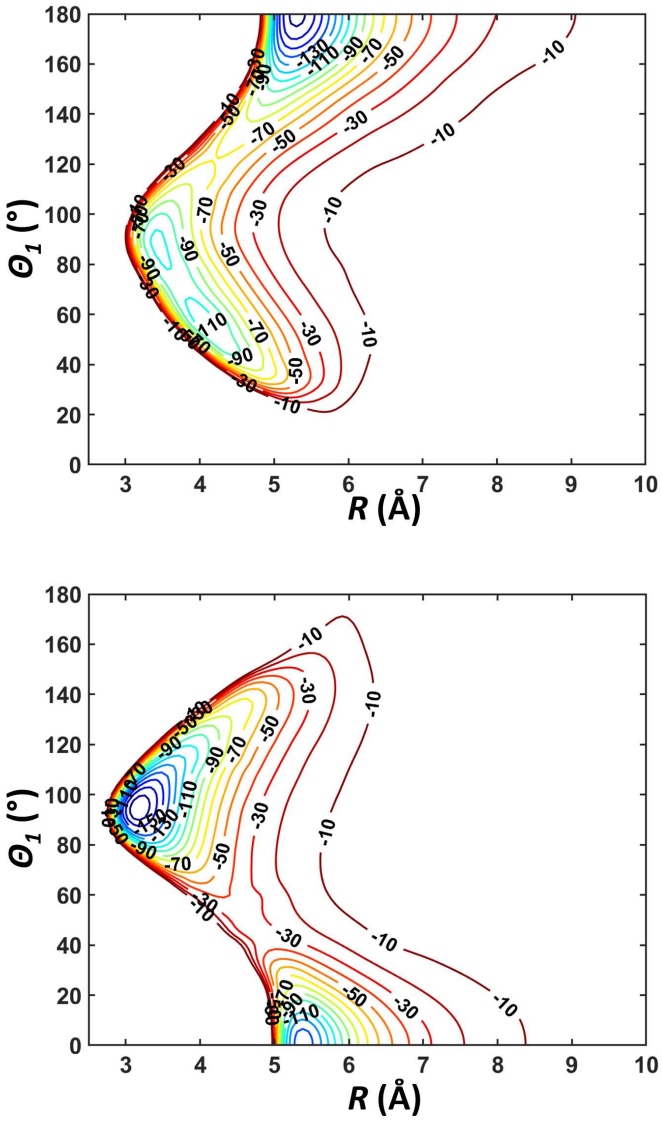

Figure 2: Plots of the highly anisotropic interaction potential for HC_2NC with H_2. (Upper panel) Plot of the end-on approach ($\theta_2 = 0°$) of H_2 fragment as a function of intermonomer distance R and orientation of HC_2NC illustrates the collinear well for approach of H_2 to the C-atom end ($\theta_1 = 180°$, see text). (Lower panel) Side-on approach ($\theta_2 = 90°$, $\phi = 0°$) of H_2 locates the global minimum for a near side-by-side arrangement (see text).

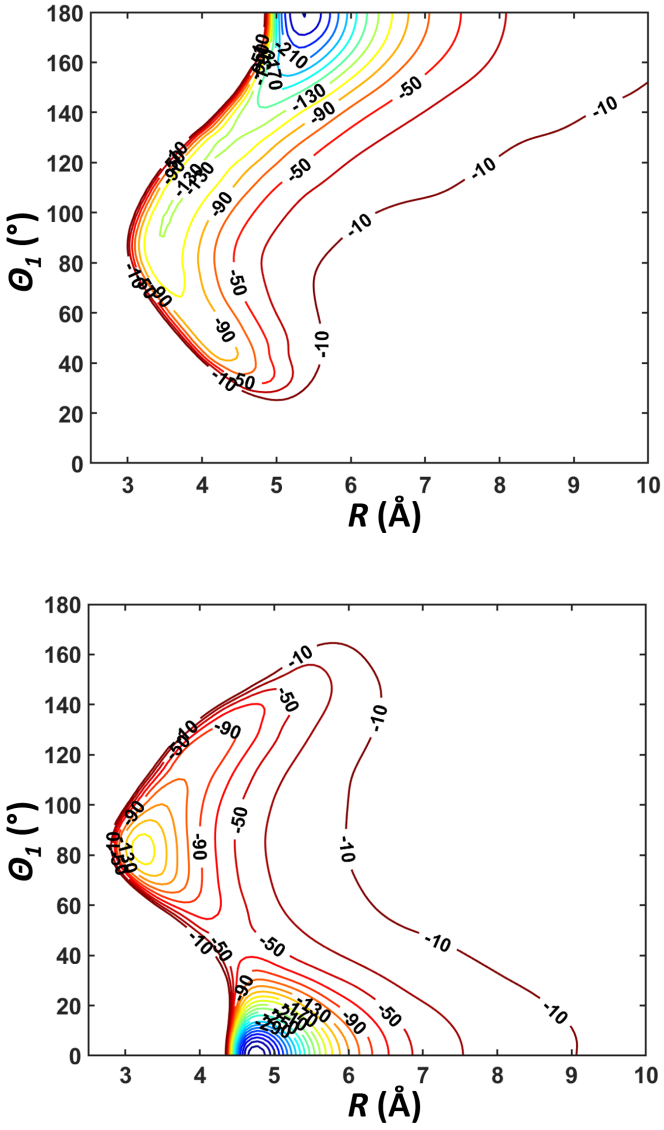

Figure 3: Plots of the highly anisotropic interaction potential for HNC_3 with H_2. (Upper panel) Plot of the end-on approach ($\theta_2 = 0°$) of H_2 fragment as a function of intermonomer distance R and orientation of HNC_3 illustrates the collinear well for approach of H_2 to the C-atom end ($\theta_1 = 0°$, see text). (Lower panel) Side-on approach of H_2 locates the global minimum for a side-on approach ($\theta_2 = 90°$, $\phi = 0°$) to the H-atom end of HNC_3 (see text).

mean-squared fitting error tolerance was set to 0.33 cm^{-1} and the total numbers of symmetry unique points needed to reach that target were 6095 for HC_2NC and 4172 for HNC_3. The maximum repulsive energy included in each fit was 2100 cm^{-1}. The contour plots in Figures 2 and 3 show the anisotropy of the interaction with respect to the HC_2NC and HNC_3 rotations, respectively, for end-on and side on approaches of H_2 fragment.

Since quantum scattering calculations require an expansion of the angular dependence of the PES into products of spherical harmonics, the 4D IMLS potential of each isomer was refitted. In terms of the Jacobi coordinates θ_1, θ_2 and ϕ, the angular expansion can be written as:

$$V(R, \theta_1, \theta_2, \phi) = \sum_{l_1, l_2, l} v_{l_1, l_2, l}(R) s_{l1, l2, l}(\theta_1, \theta_2, \phi), \quad (1)$$

where the basis functions $s_{l_1,l_2,l}$ are products of associated Legendre polynomials and cosine functions[26]. Because the PESs are highly anisotropic, the regularization procedure of Wernli *et al.*[10] was applied by scaling each IMLS PES when it is higher than a prescribed threshold so that the potential smoothly saturates to a maximum value of 665 cm^{-1}. The expansion coefficients $v_{l_1,l_2,l}$ were obtained through a least-squares fit on a random grid of 10000 angular geometries at each intermolecular separation in the range $R = 2.6 - 15.9$ Å. For HC_2NC–H_2, the expansion functions were selected iteratively using a Monte-Carlo error estimator, as described in Rist & Faure.[27] The final expansion included 380 angular terms with anisotropies up to $l_1 = 30, l_2 = 10, l = 40$. The same expansion was used for the HNC_3–H_2 system. The rms error was found to be lower than 1 cm^{-1} for intermolecular separations $R > 4.8$ Å. At lower separations, the rms increases to a few cm^{-1} due to the huge anisotropy and highly repulsive regions but the fit is still within $1 - 2$ cm^{-1} of the IMLS potential in the global minima, for both isomers. A cubic spline interpolation was finally employed over the range $R = 2.6 - 15.9$ Å and it was smooothly connected to exponential and power-law extrapolations at short and long-range, respectively. We note that non-vanishing terms beyond 15.9 Å correspond to the isotropic, dipole-quadrupole and octupole-quadrupole interaction terms.

3 Scattering calculations

In this paper, we investigate the following inelastic collision processes:

$$HC_2NC(j_1) + p{-}H_2(j_2 = 0) \rightarrow HC_2NC(j_1') + p{-}H_2(j_2' = 0) \quad (2)$$

$$HNC_3(j_1) + p{-}H_2(j_2 = 0) \rightarrow HNC_3(j_1') + p{-}H_2(j_2' = 0) \quad (3)$$

where j_1 and j_2 represent the rotational energy levels of HC_2NC (HNC_3) and H_2, respectively. Note that the para–ortho-H_2 conversion is forbidden during the collisions. The hyperfine structure of the HC_2N and HNC_3 molecules is neglected in these calculations but can be considered through from the present data using recoupling techniques as described by Lanza *et al.*[28]

We made use of the new 4D HC_2N–H_2 and HNC_3–H_2 PESs to determine rotational excitation and de-excitation cross sections between the first rotational levels of HC_2NC and HNC_3. Both HC_2NC and HNC_3 molecules were taken as rigid linear rotors with the rotational constants $B_0 = 0.1657$ cm^{-1} for HC_2NC and $B_0 = 0.1557$ cm^{-1} for HNC_3.[29]

The standard time-independent coupled scattering equations were solved using the MOLSCAT code.[30] The almost exact Close Coupling (CC) approach[26] was used. Calculations were performed for total (kinetic plus internal) energies up to 100 cm^{-1} for collisions of HC_2NC and HNC_3 with para-H_2. The integration parameters were selected to ensure convergence of the cross sections over all of the energy range. Generally, the integration range extended from 2 to at least 25 Å and the STEPS parameter allows one to constrain the step length of the integrator below 0.1 Å. The HC_2NC and HNC_3 rotational basis were sufficiently extended to ensure convergence of the inelastic cross sections. At the largest total energy considered the HC_2NC and HNC_3 rotational basis were extended to $j_1 = 33$ and $j_1 = 34$ respectively, to ensure convergence of the first 16 (up to $j_1 = 15$) rotational levels. The rotational basis of p-H_2 included only the $j_2 = 0$ levels. The level $j_2 = 2$ of p-H_2 was neglected because it was found to affect the cross-sections by less than 10–20 per cent on average while the CPU cost

was increased by large factors. The maximum value of the total angular momentum J used in the calculations was set large enough so that the inelastic cross sections were converged to within 0.05 Å^2.

From the inelastic cross sections $\sigma_{j_1 j_2 \to j_1' j_2'}(E_c)$, we have obtained the corresponding thermal rate coefficients at temperature T by a Boltzmann average over the collision energy (E_c):

$$k_{j_1 j_2 \to j_1' j_2'}(T) = \left(\frac{8}{\pi \mu {k_B}^3 T^3}\right)^{\frac{1}{2}} \times \int_0^\infty \sigma_{j_1 j_2 \to j_1' j_2'} E_c \, e^{-E_c/k_B T} \, dE_c \quad (4)$$

where k_B is Boltzmann's constant. Calculations up to the kinetic energy of 100 cm^{-1} allow us to determine rate coefficients up to 20 K. The complete set of (de-)excitation rate coefficients will be made available through the LAMDA[31] and BASECOL[32] databases.

4 Results

We have calculated the energy dependence of the collisional (de-)excitation cross sections using the computational scheme described above for transitions between the first 16 ($j = 0 - 15$) rotational levels of HC_2NC and HNC_3. The representative variation with kinetic energy of the cross sections is illustrated in Figure 4.

The de-excitation cross sections are almost monotonically decreasing functions of the energy. At low collision energies, many resonances are found. These are a consequence of the quasibound states arising from tunneling through the centrifugal energy barrier (shape resonances), or from the presence of an attractive potential well that allows the H_2 molecule to be temporarily trapped into the well and hence quasibound states to be formed (Feshbach resonances) before the complex dissociates.[33] Because of the averaging over collision energy, Eq. (4), these narrow resonances will have little, if any, effect on the relaxation rate

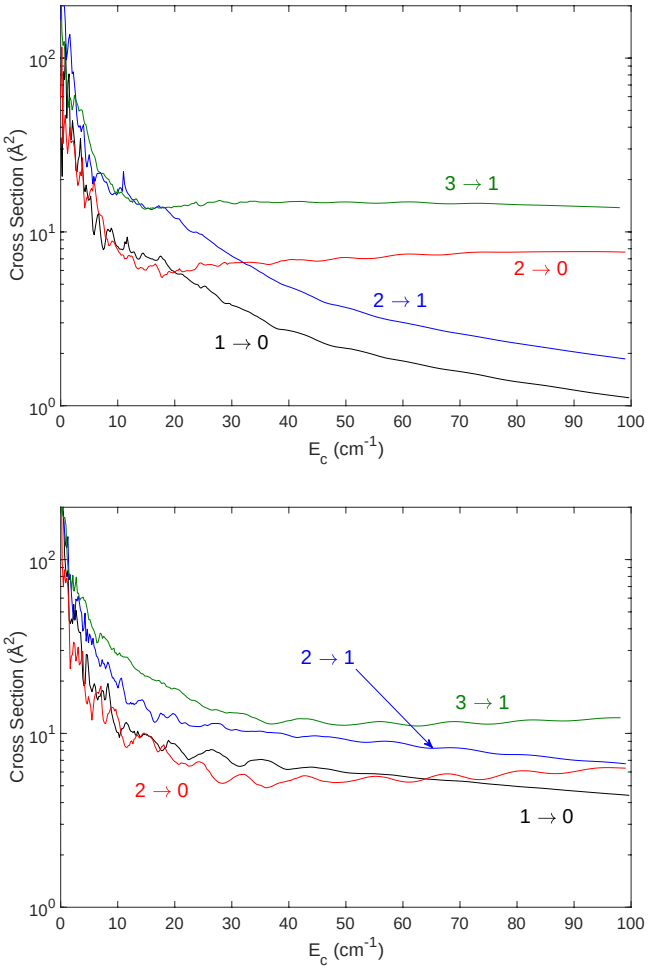

Figure 4: Typical rotational de-excitation cross-sections for the HC_2NC (upper panel) and HNC_3 (lower panel) molecules in collision with p-H_2 as a function of the collision energy.

coefficients.

We also observe that, for HC_2NC–H_2, the transitions with $\Delta j_1 = 2$ dominate over those with $\Delta j_1 = 1$ for collision energies above 30 cm^{-1}. For HNC_3–H_2 collisions, the dominance of transitions with $\Delta j_1 = 2$ over those with $\Delta j_1 = 1$ is less pronounced but exist, especially at the highest collision energies explored in this work. Such propensity can be attributed to a weak odd anisotropy in the HC_2NC–H_2 and HNC_3–H_2 PESs. Such propensity rules were also observed for the HC_3N–H_2 collisional system[9] as well as for many carbon chains such as C_2H[34,35] or C_6H.[36] The dominance of $\Delta j_1 = 2$ transitions over $\Delta j_1 = 1$ transitions is more pronounced in the case of HC_2NC than in the case of HNC_3. This can be explained by a weaker odd anisotropy in the HC_2NC–H_2 PES than in the HNC_3–H_2 PES leading to very weak $v_{l_1,l_2,l}(R)$ radial coefficients with odd l_1. However, we note that at low collision energy ($E_c < 20$ cm^{-1}), no clear propensity rules can be extracted because the behavior or the cross sections is fully dominated by resonances.

We obtained, by energy averaging of the cross sections, de-excitation rate coefficients for the first 16 ($j = 0 - 15$) rotational levels of HC_2NC and HNC_3. The representative variation with temperature is illustrated in Fig. 5.

No clear propensity rules exist for the two systems at the low temperatures considered here. Indeed, rate coefficients below 20 K are significantly influenced by the very low collision energy regime of the cross sections which are fully dominated by resonances. However, we can note that the propensity in favor of $\Delta j_1 = 2$ transitions over the $\Delta j_1 = 1$ transitions increases with increasing rotational state j_1 and is obvious for transitions from high rotational states (see Fig. 6), the dominance of the $\Delta j_1 = 2$ transitions over the $\Delta j_1 = 1$ transitions being more pronounced for the HC_2NC–H_2 collisional system than for the HNC_3NC–H_2 one. We note that these propensity rules should be different for collisions with ortho-H_2, as found in the HC_3N-H_2 system.[9]

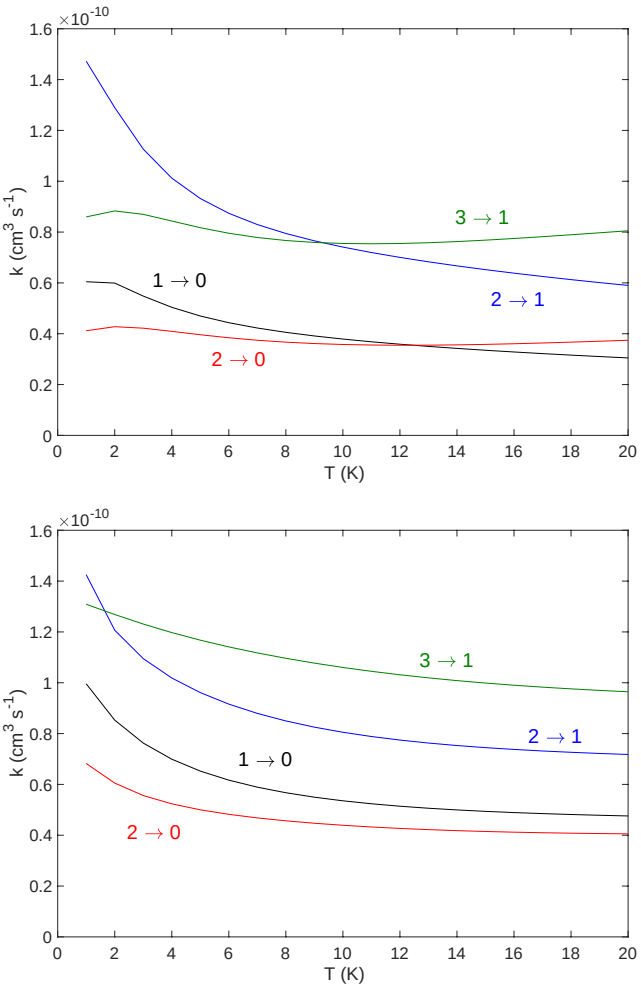

Figure 5: Typical rate coefficients for the HC_2NC (upper panel) and HNC_3 (lower panel) molecules in collision with p-H_2 as a function of the collision energy.

5 Discussion and Conclusion

We have presented the first PESs for the HC_2NC–H_2 and HNC_3–H_2 collisional systems. Both *ab initio* data were computed at the CCSD(T)-F12b level of theory. 4D PESs were constructed using the IMLS method. We furthermore performed inelastic scattering calculations on these surfaces in order to describe the collisions of HC_2NC and HNC_3 with para-H_2 for low internal excitations of HC_2NC and HNC_3.

In the absence of available collisional data for the HC_2NC and HNC_3 molecules, rate coefficients from only HC_3N could have been used to model the observations of both isomers in molecular clouds. In order to check the validity of such an approach and more generally the impact of isomerism effects in the collisional excitation studies, we have compared HC_3N, HC_2NC and HNC_3 rate coefficients. Figure 6 shows the HC_3N, HC_2NC and HNC_3 de-excitation rate coefficients from the $j_1 = 10$ level due to para-H_2 collisions at 10 K.

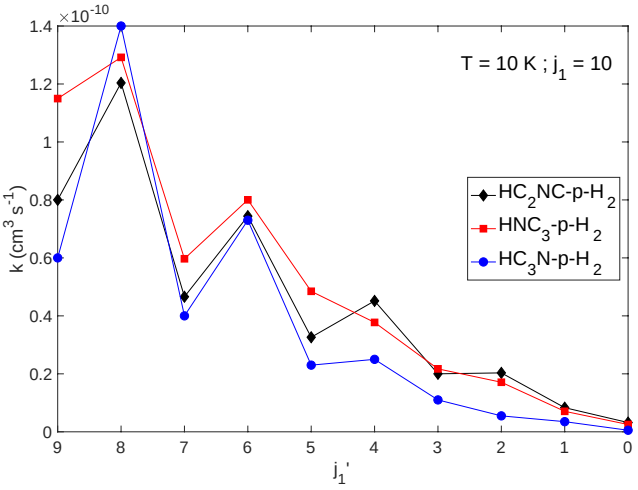

Figure 6: HC_3N–H_2, HC_2NC–H_2 and HNC_3–H_2 de-excitation rate coefficients from the initial level $j_1 = 10$ at 10 K.

All the collisional systems exhibit the same propensity rules in favor of $\Delta j_1 = 2$ transition. Nevertheless, we note that the rate coefficients for the $\Delta j_1 = 1$ transitions are significantly different, the rate coefficient for HNC_3 being almost two times larger than that of HC_3N. Differences are also found for the other transitions but they are more limited. Such differences

originate from the differences seen in the PESs. Indeed, as discussed above, the PESs of the different isomers differ by the shape and the well-depth resulting in significant differences in the magnitude of the rate coefficients.

Hence, the present comparison confirms that actual rate coefficients should be obtained for each of the different isomers and confirms previous findings on isomerism effects found with other cyanides and isocyanides like AlCN/AlNC, MgCN/MgNC or HCN/HNC.

We note that all three isomers have been detected in the TMC-1 dark cloud[4,5] and the prestellar core L1544,[37] with abundance ratios HC_3N:HC_2NC:$HNC_3 \sim 500 : 7.5 : 1$ in TMC-1 and $\sim 200 : 10 : 1$ in L1544. These ratios significantly deviate from thermodynamic equilibrium at ~ 10 K, as expected when the chemistry is under kinetic control. Still, the relative abundances are in agreement with the relative energies. Isomer abundance ratios are very important to understand the dominant formations pathways in the ISM. A detailed modeling of the chemistry of HC_3N isomers can be found in the recent work of Vastel *et al.*[37] The analysis of the observations, however, were so far performed within the LTE hypothesis due to the lack of collisional rate coefficients for HC_2NC and HNC_3. The present data will help to derive more accurate abundance ratios through non-LTE modeling and therefore to improve our understanding of relative isomer populations. In particular, as the different isomers exhibit different excitation conditions, we anticipate that the LTE approximation used in previous work will not impact the abundance of the isomers homogeneously. A revision of the HC_3N:HC_2NC:HNC_3 abundance ratio could then be anticipated. An accurate determination of such ratio will put more constraints on the understanding of nitrogen chemistry in the ISM that is still only partly understood.

Finally, the present calculations will be extended to higher rotational levels and temperature to cover the astrophysical needs, especially for the interpretation of the observations of warm ISM and circumstellar gas. In these calculations, collisions with orho-H_2 will be considered as it can be a primary collisional partner in such regions.

Acknowledgement

RD and EQS are supported by the US National Science Foundation (No. CHE-1566246). F.L. acknowledges financial support from the Institut Universitaire de France and from the French National Research Agency (ANR) through a grant to the Anion Cos Chem project (ANR-14-CE33-0013). We acknowledge the Programme National "Physique et Chimie du Milieu Interstellaire" (PCMI) of CNRS/INSU with INC/INP co-funded by CEA and CNES.

References

(1) Turner, B. E. Detection of interstellar cyanoacetylene. *Astrophysical Journal, Letters* **1971**, *163*, L35.

(2) Cordiner, M. A.; Charnley, S. B.; Wirström, E. S.; Smith, R. G. Organic chemistry of low-mass star-forming cores. I. 7 mm spectroscopy of chamaeleon MMS1. *Astrophysical Journal* **2012**, *744*, 131.

(3) Cordiner, M. A.; Buckle, J. V.; Wirström, E. S.; Olofsson, A. O. H.; Charnley, S. B. On the ubiquity of molecular anions in the dense interstellar medium. *Astrophysical Journal* **2013**, *770*, 48.

(4) Kawaguchi, K.; Ohishi, M.; Ishikawa, S.-I.; Kaifu, N. Detection of isocyanoacetylene HCCNC in TMC-1. *Astrophysical Journal, Letters* **1992**, *386*, L51–L53.

(5) Kawaguchi, K.; Takano, S.; Ohishi, M.; Ishikawa, S.-I.; Miyazawa, K.; Kaifu, N.; Yamashita, K.; Yamamoto, S.; Saito, S.; Ohshima, Y.; Endo, Y. Detection of HNCCC in TMC-1. *Astrophysical Journal, Letters* **1992**, *396*, L49–L51.

(6) Gensheimer, P. D. Observations of HCCNC and HNCCC in IRC+10216. *Astrophysics and Space Science* **1997**, *251*, 199–202.

(7) Loison, J.-C.; Wakelam, V.; Hickson, K. M. The interstellar gas-phase chemistry of HCN and HNC. *Monthly Notices of the Royal Astronomical Society* **2014**, *443*, 398–410.

(8) Roueff, E.; Lique, F. Molecular excitation in the interstellar medium: recent advances in collisional, radiative, and chemical processes. *Chem. Rev.* **2013**, *113*, 8906–8938.

(9) Faure, A.; Lique, F.; Wiesenfeld, L. Collisional excitation of HC_3N by para- and ortho-H_2. *Monthly Notices of the Royal Astronomical Society* **2016**, *460*, 2103–2109.

(10) Wernli, M.; Wiesenfeld, L.; Faure, A.; Valiron, P. Rotational excitation of HC_3N by H_2 and He at low temperatures. *Astronomy and Astrophysics* **2007**, *475*, 391–391.

(11) Sarrasin, E.; Abdallah, D. B.; Wernli, M.; Faure, A.; Cernicharo, J.; Lique, F. The rotational excitation of HCN and HNC by He: new insights on the HCN/HNC abundance ratio in molecular clouds. *MNRAS* **2010**, *404*, 518–526.

(12) Hernández Vera, M.; Lique, F.; Dumouchel, F.; Kłos, J.; Rubayo Soneira, J.; Senent, M.-L. Cyanide/isocyanide abundances in the interstellar medium - II. Inelastic rate coefficients of Al and Mg compounds. *Monthly Notices of the Royal Astronomical Society* **2013**, *432*, 468–477.

(13) Hernández Vera, M.; Lique, F.; Kłos, J.; Dumouchel, F.; Rubayo Soneira, J. Cyanides/isocyanides abundances in the interstellar medium - IV. Temperature dependence of SiCN/SiNC rate coefficients and astrophysical applications. *Monthly Notices of the Royal Astronomical Society* **2015**, *451*, 1199–1211.

(14) Hernández Vera, M.; Lique, F.; Dumouchel, F.; Hily-Blant, P.; Faure, A. The rotational excitation of the HCN and HNC molecules by H_2 revisited. *Monthly Notices of the Royal Astronomical Society* **2017**, *468*, 1084–1091.

(15) Nguyen, T. L.; Baraban, J. H.; Ruscic, B.; Stanton, J. F. On the HCN–HNC Energy Difference. *The Journal of Physical Chemistry A* **2015**, *119*, 10929–10934.

(16) Adler, T. B.; Knizia, G.; Werner, H. A simple and efficient CCSD(T)-F12 approximation. *Journal of Chemical Physics* **2007**, *127*, 221106–+.

(17) Botschwina, P.; Horn, M.; Seeger, S.; Flügge, J. A theoretical investigation of HC_2NC and HNC_3. *Chemical Physics Letters* **1992**, *195*, 427–434.

(18) Hill, J. G.; Mazumder, S.; Peterson, K. A. Correlation consistent basis sets for molecular core-valence effects with explicitly correlated wave functions: The atoms B-Ne and Al-Ar. *Journal of Chemical Physics* **2010**, *132*, 054108.

(19) Werner, H.-J.; Knowles, P. J.; Knizia, G.; Manby, F. R.; Schütz, M. Molpro: a general-purpose quantum chemistry program package. *Wiley Interdisciplinary Reviews: Computational Molecular Science* **2012**, *2*, 242–253.

(20) Donoghue, G.; Wang, X.-G.; Dawes, R.; Carrington Jr, T. Computational study of the rovibrational spectra of CO_2–C_2H_2 and CO_2–C_2D_2. *Journal of Molecular Spectroscopy* **2016**, *330*, 170–178.

(21) Wang, X.-G.; Carrington Jr, T.; Dawes, R. Computational study of the rovibrational spectrum of $(CO_2)_2$. *Journal of Molecular Spectroscopy* **2016**, *330*, 179–187.

(22) Brown, J.; Wang, X.-G.; Carrington Jr, T.; Grubbs, G. S.; Dawes, R. Computational study of the rovibrational spectrum of CO_2–CS_2. *The Journal of chemical physics* **2014**, *140*, 114303.

(23) Dawes, R.; Quintas-Sánchez, E. The Construction of ab initio-based potential energy surfaces. *Rev. Comput. Chem* **2018**, *31*, 199–264.

(24) Quintas-Sánchez, E.; Dawes, R. AUTOSURF: A freely available program to construct

potential energy surfaces. *Journal of chemical information and modeling* **2019**, *59*, 262–271.

(25) Majumder, M.; Ndengue, S. A.; Dawes, R. Automated construction of potential energy surfaces. *Mol. Phys.* **2016**, *114*, 1–18.

(26) Green, S. Rotational excitation in H_2–H_2 collisions - Close-coupling calculations. *Journal of Chemical Physics* **1975**, *62*, 2271–2277.

(27) Rist, C.; Faure, A. A Monte Carlo error estimator for the expansion of rigid-rotor potential energy surfaces. *Journal of Mathematical Chemistry* **2012**, *50*, 588–601.

(28) Lanza, M.; Lique, F. Hyperfine excitation of linear molecules by para- and ortho-H_2: Application to the HCl-H_2 system. *Journal of Chemical Physics* **2014**, *141*, 164321.

(29) Huber, K. P.; Herzberg, G. *Molecular spectra and molecular structure. IV. Constants of diatomic molecules*; Van Nostrand Reinhold: New York, 1979.

(30) Hutson, J. M.; Green, S. 1994; MOLSCAT computer code, version 14 (1994), distributed by Collaborative Computational Project No. 6 of the Engineering and Physical Sciences Research Council (UK).

(31) Schöier, F. L.; van der Tak, F. F. S.; van Dishoeck, E. F.; Black, J. H. An atomic and molecular database for analysis of submillimetre line observations. *Astron. Astrophys.* **2005**, *432*, 369–379.

(32) Dubernet, M. L. et al. BASECOL2012: A collisional database repository and web service within the Virtual Atomic and Molecular Data Centre (VAMDC). *Astronomy and Astrophysics* **2013**, *553*, A50.

(33) Smith, L. N.; Malik, D. J.; Secrest, D. Rotational compound state resonances for an argon and methane scattering system. *Journal of Chemical Physics* **1979**, *71*, 4502–4514.

(34) Dumouchel, F.; Lique, F.; Spielfiedel, A.; Feautrier, N. Hyperfine excitation of C_2H and C_2D by para-H_2. *Monthly Notices of the Royal Astronomical Society* **2017**, *471*, 1849–1855.

(35) Dagdigian, P. J. Hyperfine excitation of C_2H in collisions with ortho- and para-H_2. *Monthly Notices of the Royal Astronomical Society* **2018**, *479*, 3227–3231.

(36) Walker, K. M.; Lique, F.; Dawes, R. Fine and hyperfine collisional excitation of C_6H by He. *Monthly Notices of the Royal Astronomical Society* **2018**, *473*, 1407–1415.

(37) Vastel, C.; Kawaguchi, K.; Quénard, D.; Ohishi, M.; Lefloch, B.; Bachiller, R.; Müller, H. S. P. High spectral resolution observations of HNC_3 and HCCNC in the L1544 pre-stellar core. *Monthly Notices of the Royal Astronomical Society* **2018**, *474*, L76–L80.

Graphical TOC Entry